Attosecond Optical Switching

Dandan Hui
University of Arizona
Husain Alqattan
University of Arizona
Simin Zhang
Ohio State University
Vladimir Pervak
Ludwig-Maximilians-Universität München
Enam Chowdhury
The Ohio State University
Mohammed Hassan (mohammedhassan@email.arizona.edu)
University of Arizona https://orcid.org/0000-0002-9669-534X

Article

Keywords:

Posted Date: January 28th, 2022

DOI: https://doi.org/10.21203/rs.3.rs-1232650/v1

Title

Attosecond Optical Switching

Author list

Dandan Hui[1†], Husain Alqattan[1†], Simin Zhang[2], Vladimir Pervak[3], Enam Chowdhury[2], Mohammed Th. Hassan[*1].

Affiliations

[1] Department of Physics, University of Arizona, Tucson, AZ 85721, USA.

[2] Department of Material Science and Engineering, The Ohio State University, Columbus, OH 43210, USA.

[3] Ludwig-Maximilians-Universität München, Am Coulombwall 1, 85748, Garching, Germany.

*Correspondence to: mohammedhassan@arizona.edu

†These authors contributed equally to this work.

Abstract

Modern electronics are founded on switching the electric signal by radio frequency (RF) electromagnetic fields on the nanosecond timescale, limiting the information processing to the gigahertz speed. Recently, optical switches have been demonstrated using terahertz and ultrafast laser pulses to control the electric signal and enhance the switching speed to the picosecond and a few hundred femtoseconds time scale[1-13]. Here, we exploit the reflectivity modulation of a dielectric system in a strong light field to demonstrate the optical switching (ON/OFF) with attosecond time resolution. Moreover, we present the capability of controlling the optical switching signal with complex synthesized fields of ultrashort laser pulses for data binary encoding. This work paves the way for establishing optical switches and light-based electronics with peta- and exahertz speeds, several orders of magnitude faster than the current semiconductor-based electronics, opening a new realm in information technology, optical communications, and photonic processor technologies.

Main

The strong ultrafast laser pulses induce phase transition in dielectric material due to strong field interaction [14-20]. The charge carriers are excited from the valance band to the conduction band in the dielectric via multiphoton excitation[20]. Then, the excited electrons in the conduction band move in the reciprocal space by acquiring a time-dependent momentum from the driving field[14,19-21]. Hence, the electrons are accelerated and decelerated following the shape of the driver field's vector potential, causing an instantaneous modulation in the electronic structure of the dielectric system[14,21-23].

Consequently, the dielectric undergoes an instantaneous phase transition, causing alternations in the dielectric constant and the optical properties of the system due to the strong polarizability[17,24]. Hence, the reflectivity of the fused silica modulates following the driver field[20], enabling the control of the material and its optical properties in real-time. In this work, we demonstrate the attosecond optical switching exploiting the oscillation of the dielectric material reflectivity from maximum to minimum in a half field-cycle time scale as illustrated in Fig. 1. Accordingly, the reflected light signal is switching from ON to OFF with sub-femtosecond resolution. Moreover, using complex synthesized light field waveforms to alter the reflectivity of the dielectric enables one to control the switching signal and allows the digital binary encoding with the exahertz speed.

In our experiment, we use a synthesized light waveform generated by the attosecond light field synthesizer (ALFS)[25](pulse duration=2.7 fs) with a nominal carrier wavelength = 550 nm to modify the fused silica reflectivity, which is probed by another weak light field (probe pulse), as explained in the Method section. The reflected probe beam spectrum is recorded as a function of the time delay between the pump and probe pulses (Fig. 1). The measured spectrogram (average of three scans) —depicted in Fig. 2a—shows the reflected probe beam (off the fused silica front surface) spectrum in the real-time. The reflectivity modulation is frequency and time dependent which is distinctly observed by subtracting the reflected probe spectrum in the absence of the

driver field as shown in the spectrogram in Fig. 2b. Hence, the reflectivity switches from maximum (ON) to a minimum (OFF) in sub-femtosecond (900 as) time scale. The integration of the measured spectra amplitude as a function of time delay—total reflectivity modulation (TRM) trace (Fig. 2c) —gives an access to the vector potential, and the driver field (Extended Data Fig. 1)[14].

At τ=0 fs, the fused silica experiences a phase transition to a semi-metal like phase, and the reflectivity increases by ~25 % (reflected spectrum of the probe beam, in this case, is shown in the red line in Fig. 2d) with respect to the reflectivity of the fused silica in the equilibrium state (reflected spectrum with no field effect shown in the black line in Fig. 2d). In contrast, at τ=0.9 fs, the reflectivity reduces by ~21 % (blue line in Fig. 2d). Hence, the reflectivity changes by a total value of ~45% in a half-cycle time scale representing the switching intensity resolution. Moreover, the measured reflected spectra in Fig. 2d show that the strong field-induced phase transition of the fused silica is reversible following the driver field oscillations direction. Note, the transmission signal of the dielectric system is also varying in the strong field, although, the transmitted light suffers nonlinear propagation and dispersion effects. Therefore, the study of the transmitted light signal is complicated, and does not solely reflect the phase transition dynamics of the system.

Henceforth, we developed a classical model (see details in the Supplementary Information) to simulate the dielectric constant and the measured fused silica

reflectivity dynamics in the presence of the strong field (using the driver field used in the experimental measurements and shown in the Extended Data Fig. 1). The reflectivity modulation $R_e(\omega)$ can be expressed as

$$R_e(\omega) = I(\omega) \times R_m(\omega) \qquad (1)$$

where $I(\omega)$ is the spectrum of the probe pulse and $R_m(\omega)$ is the modified reflectivity of fused silica regardless of the pulse spectrum. $R_m(\omega)$ can be expressed as

$$R_m(\omega) = \frac{[1-n(\omega)]^2+\kappa^2(\omega)}{[1+n(\omega)]^2+\kappa^2(\omega)}, \qquad (2)$$

where $\tilde{n} = \pm\sqrt{\tilde{\varepsilon}_r} = n(\omega) + i\kappa(\omega)$ is the refractive index, $\tilde{\varepsilon}_r$ is the relative permittivity. The measured reflectivity modulation spectrogram (Fig. 2a) is fitted using the developed model. The obtained spectrogram is shown in Fig. 3a. The calculated spectrogram after subtracting the background spectrum (the reflected spectrum at no pump shown in black line in Fig. 2d) is shown in Fig. 3b. These simulated spectrograms show the same reflectivity dynamics pattern in time and frequency domains as the measured spectrograms shown in Fig. 2a,b, with a standard deviation of ~2.5%. Also, the calculated spectra at τ=0 & 0.9 fs are extracted and plotted in the red and blue solid lines in Fig. 3c, d, respectively. The integration of these two spectra indicates that the reflectivity has increased at τ =0 fs and reduced at τ =0.9 fs by almost the same value (~20%), very close to the refelctvity change at the two time instances. The

measured and corresponding calculated reflected spectra, plotted in Fig. 3c&d, are in excellent agreement.

As demonstrated experimentally in Fig. 2, the light-induced phase transition of the fused silica allows us to switch between an ON and OFF state of the reflected light signal following the driver field. Consequently, the reflectivity modulation and the switching alterability can be controlled by tailoring the driver field waveform. Accordingly, we demonstrate next the control of the switching signals using on-demand complex synthesized waveforms generated by ALFS [25-27]. Fig. 4a (I), b (I), and c (I), show some of the measured reflectivity modulation spectrograms—after subtracting background spectrum — triggered by three different synthesized light fields. The integrated intensities of the reflected spectra at different instances of time (above zero amplitude) are plotted in Fig. 4a (II), b (II), and c (II). Note, the light signal can also be measured by a photodiode detector instead of the spectrometer to directly detect the integrated intensity signal. The light signal switches from ON to OFF states *uniformly* every half-cycle of the driver field. By setting a certain intensity amplitude threshold (60%) in Fig. 4a (II), b (II), and c (II)—which easily can be experimentally implemented or programmed in the photodetector —the number of the detected light signal (above this threshold) and the switching alternative-time varies depending on the shape of the driver waveform. Fig. 4a (III), b (III), and c (III) show the signals above the 60% threshold, and the insets in the top (contains 26 slots) represent the signal status

(OFF or ON) in black and white in real-time at each half cycle of the driver field. Using the first waveform, the signal switches ON and OFF three times with a time separation of 4.5 fs and 3.6 fs. This switching time interval is controlled to be 3.6 and 1.8 fs (as shown in Fig. 4b(II)) using the second waveform. Moreover, the number of the switching signal increases to four by using the third waveform with 2.7, 1.8, and 3.6 fs time period separations between the signals as shown in Fig. 4c (III).

Remarkably, this capability of controlling the light signal switching (ON/OFF) with attosecond resolution allows to encode data with synthesized light waveforms[25], which are beyond the reach of conventional ultrafast pulses field. Accordingly, the reflected signal above the threshold will be detected "ON status" and presents the binary code "1". The reflected signal below the threshold— will not be detected by the photodetector and hence will have an "OFF status"— representing the binary code "0". The number of coding bits that the light field can carry equals twice of the number of the driver light field cycles. Some of the examples of binary encoding using the synthesized waveforms are shown in the insets of Fig. 4a (III), b (III), and c (III).

In a potential ultrafast light field encoding process (illustrated in Extended Data Fig. 2), the data will be encoded on the synthesized light waveforms generated by the ALFS[25] (or any pulse shaping device), which will act as an "encoder" device. Then, the synthesized waveform (which is consider to be the encoded

laser beam) will carry the data from the transmitter to the receiver station. Next, the encoded laser beam will be focused on the dielectric together with another beam (decoder laser beam). Finally, the reflected decoder laser beam from the dielectric will be detected by a photodetector. After setting a certain predefined threshold, the photodetector will read the coded data in the 1 & 0 binary form. The light field encoding can be obtained using multicycle pulses, which are provided by the commercial laser systems available in the market, in combination with pulse shaping technology[25-30]. Notably, this demonstrated optical switching occurs in ambient conditions allowing a simple realistic architecture of a potentially realistic compact optical switch integrated on a photonic chip. Moreover, the data encoding on ultrafast light waveforms, in contrast to the encoding provided by modern electronic sources using a microwave, would significantly enhance the data processing and transformation speed for light-time distances.

In conclusion, the light-field induced phase transition of dielectric system in strong field enables switching the reflected light signal ON and OFF with attosecond switching speed. The light field tailoring and shaping with high resolution allow us to demonstrate the attosecond optical switching control and data binary encoding by syntehsized laser pulses. This work paves the way to develop an ultrafast optical-based switches, and to transfer data with petahertz speed and beyond, which can carry information to the deep space opening a new era in communication and information technology.

Method

Time-resolved reflected spectra measurements: A multicycle pulse carried at a central wavelength of 800 nm is focused and propagated in a Hollow-Core-Fiber (HCF) to generate a broadband spectrum that spans from Ultra-Violet (UV) to Near-Infrared (NIR) spectral regions. This supercontinuum is divided into three spectral channels and compressed inside the attosecond light field synthesizer (ALFS) apparatus[25]. At the exist of ALFS, the three channels are superimposed to generate a synthesized waveform of 2.7 fs pulse. The relative delays and intensities of the three channels inside the ALFS are controlled to synthesize complex waveforms on-demand. The carrier-envelope-phase of the synthesized waveform is passively locked to less than 100 mrad (the laser source is OPCPA based). Also, the relative phases between the three channel's pulses inside the ALFS are actively locked to ensure the waveform stability during the experiment[25]. The output beam from the ALFS is divided into two beams by passing through a two-hole mask with different hole diameters. One of the two merged beams, has a high intensity (estimated field strength is 1 V/Å), is utilized as a pump beam to alter the reflectivity of the dielectric system[14]. The second beam (probe beam) has a lower intensity (~2.5% of the pump beam intensity) so it is not inducing any reflectivity changes on the system. The two beams are focused and overlapped on the fused silica sample (thickness~100 μm) by two focusing D-shape mirrors (f=10 cm). One of the two

D-shape mirrors is attached to a high-resolution (nanometer) delay stage. The probe beam is partially reflected from the fused silica sample, then it is filtered out from the pump beam, and focused on the entrance of an optical spectrometer. The reflected probe beam's spectra are acquired as a function of the time delay between the pump and probe pulses. Moreover, The complex waveforms used to control the reflectivity and control the switching signals (shown in Fig. 4) are generated by changing the relative phase delay and intensities between the ALFS channels, more details about the light field synthesis scheme by ALFS can be found elsewhere[25].

Acknowledgments

This project is funded by the Gordon and Betty Moore Foundation Grant **GBMF7938** to M. Hassan. This material is also based upon work supported by the Air Force Office of Scientific Research under award number **FA9550-19-1-0025**.

Author Contributions:

D.H. and H.A conducted the experiments and analyzed the data. S.Z. and E.C. carried out the simulations and calculations. V.P. designed and measured the optics of the ALFS. M.H. conceived, supervised, and directed the study. All authors discussed the results and their interpretation and wrote the manuscript.

Ethics declarations

Authors declare no competing interests.

Data Availability

The datasets generated and/or analyzed during this study are available from the corresponding authors on reasonable request.

Code availability

The analysis codes that support the study's findings are available from the corresponding authors on reasonable request.

References

1 Ono, M. *et al.* Ultrafast and energy-efficient all-optical switching with graphene-loaded deep-subwavelength plasmonic waveguides. *Nature Photonics* **14**, 37-43, (2020).

2 Zasedatelev, A. V. *et al.* A room-temperature organic polariton transistor. *Nature Photonics* **13**, 378-383, (2019).

3 Nozaki, K. *et al.* Sub-femtojoule all-optical switching using a photonic-crystal nanocavity. *Nature Photonics* **4**, 477-483, (2010).

4 Yang, Y. *et al.* Femtosecond optical polarization switching using a cadmium oxide-based perfect absorber. *Nature Photonics* **11**, 390-395, (2017).

5 Li, W. *et al.* Ultrafast all-optical graphene modulator. *Nano letters* **14**, 955-959, (2014).

6 Takahashi, R., Itoh, H. & Iwamura, H. Ultrafast high-contrast all-optical switching using spin polarization in low-temperature-grown multiple quantum wells. *Applied Physics Letters* **77**, 2958-2960, (2000).

7 Tan, W., Ma, J., Zheng, Y. & Tong, J. Femtosecond optical Kerr gate with double gate pulses. *IEEE Photonics Technology Letters* **30**, 266-269, (2017).

8 Liu, Y. *et al.* 10 fs ultrafast all-optical switching in polystyrene nonlinear photonic crystals. *Applied Physics Letters* **95**, 131116, (2009).

9 Hirao, K., Mitsuyu, T., Si, J. & Qiu, J. *Active glass for photonic devices: photoinduced structures and their application*. Vol. 7 (Springer Science & Business Media, 2013).

10 Iizuka, N., Kaneko, K. & Suzuki, N. All-optical switch utilizing intersubband transition in GaN quantum wells. *IEEE journal of quantum electronics* **42**, 765-771, (2006).

11 Sethi, P. & Roy, S. All-optical ultrafast XOR/XNOR logic gates, binary counter, and double-bit comparator with silicon microring resonators. *Applied optics* **53**, 6527-6536, (2014).

12 Zhang, Q. *et al.* Ultrafast optical Kerr effect of Ag–BaO composite thin films. *Applied physics letters* **82**, 958-960, (2003).

13 Li, Y., Bhattacharyya, A., Thomidis, C., Moustakas, T. D. & Paiella, R. Ultrafast all-optical switching with low saturation energy via intersubband transitions in GaN/AlN quantum-well waveguides. *Optics Express* **15**, 17922-17927, (2007).

14 Hui, D. *et al.* Attosecond electron motion control in dielectric. *Nature Photonics*, (2021).

15 Schultze, M. *et al.* Controlling dielectrics with the electric field of light. *Nature* **493**, 75-78, (2013).

16 Apalkov, V. & Stockman, M. I. Theory of dielectric nanofilms in strong ultrafast optical fields. *Physical Review B* **86**, 165118, (2012).
17 Wachter, G. *et al.* Ab initio simulation of electrical currents induced by ultrafast laser excitation of dielectric materials. *Physical review letters* **113**, 087401, (2014).
18 Glezer, E., Siegal, Y., Huang, L. & Mazur, E. Laser-induced band-gap collapse in GaAs. *Physical Review B* **51**, 6959, (1995).
19 Schiffrin, A. *et al.* Optical-field-induced current in dielectrics. *Nature* **493**, 70-74, (2013).
20 Khurgin, J. B. Optically induced currents in dielectrics and semiconductors as a nonlinear optical effect. *JOSA B* **33**, C1-C9, (2016).
21 Paasch-Colberg, T. *et al.* Sub-cycle optical control of current in a semiconductor: from the multiphoton to the tunneling regime. *Optica* **3**, 1358-1361, (2016).
22 Sederberg, S. *et al.* Attosecond optoelectronic field measurement in solids. *Nature communications* **11**, 1-8, (2020).
23 Korobenko, A. *et al.* Femtosecond streaking in ambient air. *Optica* **7**, 1372-1376, (2020).
24 Yabana, K., Sugiyama, T., Shinohara, Y., Otobe, T. & Bertsch, G. Time-dependent density functional theory for strong electromagnetic fields in crystalline solids. *Physical Review B* **85**, 045134, (2012).
25 Alqattan, H., Hui, D., Pervak, V. & Hassan, M. T. Attosecond light field synthesis for electron motion control. *arXiv:2112.10700*, (2021).
26 Hassan, M. T. *et al.* Optical attosecond pulses and tracking the nonlinear response of bound electrons. *Nature* **530**, 66-70, (2016).
27 Hassan, M. T. *et al.* Invited Article: Attosecond photonics: Synthesis and control of light transients. *Review of Scientific Instruments* **83**, 111301, (2012).
28 Weiner, A. M. Ultrafast optical pulse shaping: A tutorial review. *Optics Communications* **284**, 3669-3692, (2011).
29 Cundiff, S. T. & Weiner, A. M. Optical arbitrary waveform generation. *Nature Photonics* **4**, 760-766, (2010).
30 Wirth, A. *et al.* Synthesized Light Transients. *Science* **334**, 195-200, (2011).

Figures and Figure legends

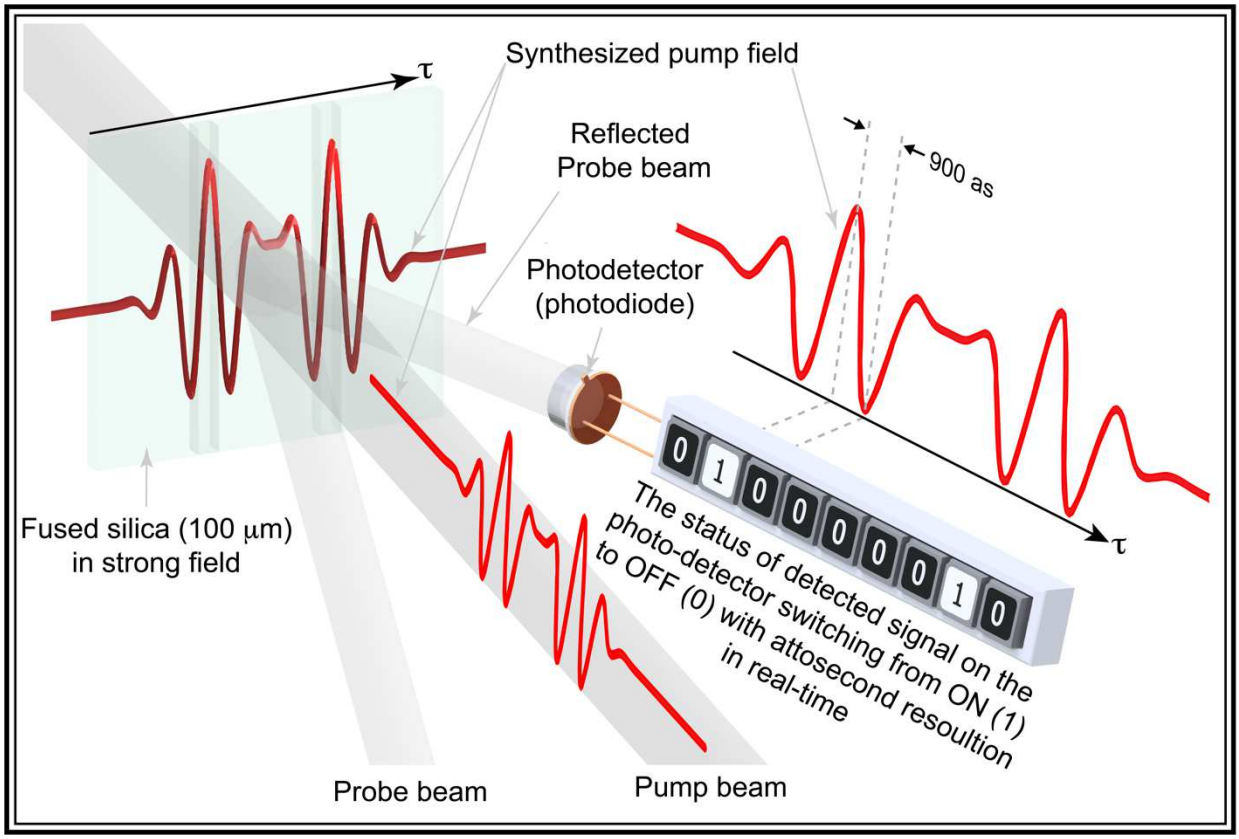

Fig. 1 | The basic principle of the attosecond optical switching based on strong field interaction with dielectric. The pump light field induces the instantaneous phase transition in the dielectric (fused silica) system and causes the change in the reflectivity of the dielectric following the shape of the incident pump pulse waveform in real-time. The reflectivity modification is detected by measuring the reflected probe beam's change using a photodetector (e.g., photodiode) as a function of the time delay between pump and probe beams. The detected reflected signal is switched OFF/ON (presented by 0/1), depending on the field intensity at the time τ, in the real-time. The switching resolution is equal to the duration of the half-cycle field (900 as) of the pump pulse and can be controlled by tailoring the pump field waveform using the attosecond light field synthesis approach. The attosecond optical switching and control allow to encode data on ultrafast laser pulse and open the door for establishing the ultrafast optical switchs.

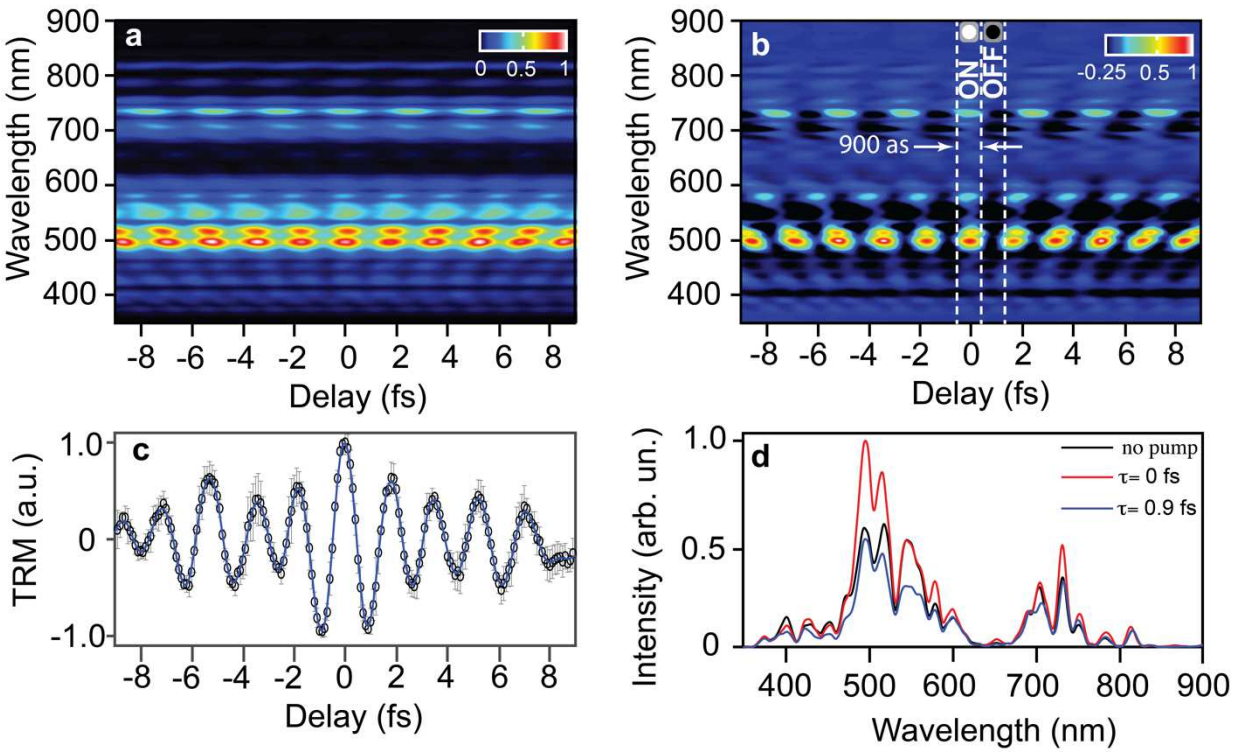

Fig. 2 | Attosecond optical switching. The reflectivity of SiO_2 is modulated in real-time due to the interaction with a strong (pump) light field. **a**, The measured spectrogram (average three scans) of the reflected probe beam as a function of the time delay between the pump and probe pulses. **b**, The obtained spectrogram by subtracting the probe spectrum in the absence of pump field from the measured spectrogram (shown in a). The reflectivity switches between maximum to minimum alternatively in 900 attosecond time scale. **c**, The normalized total reflectivity modulation (TRM) of the SiO_2 in the strong field retrieved obtained from the measured spectrogram (in a) by the integration of the probe spectrum at each instance of time. **d**, The probe beam's spectrum reflected from the SiO_2 in the equilibrium state (in the absence of pump field) is shown in the black line. In contrast, reflected spectra intensities of the probe beam (outlined from the spectrogram in **a)** at τ=0 & 0.9 fs are plotted in red and blue lines, respectively.

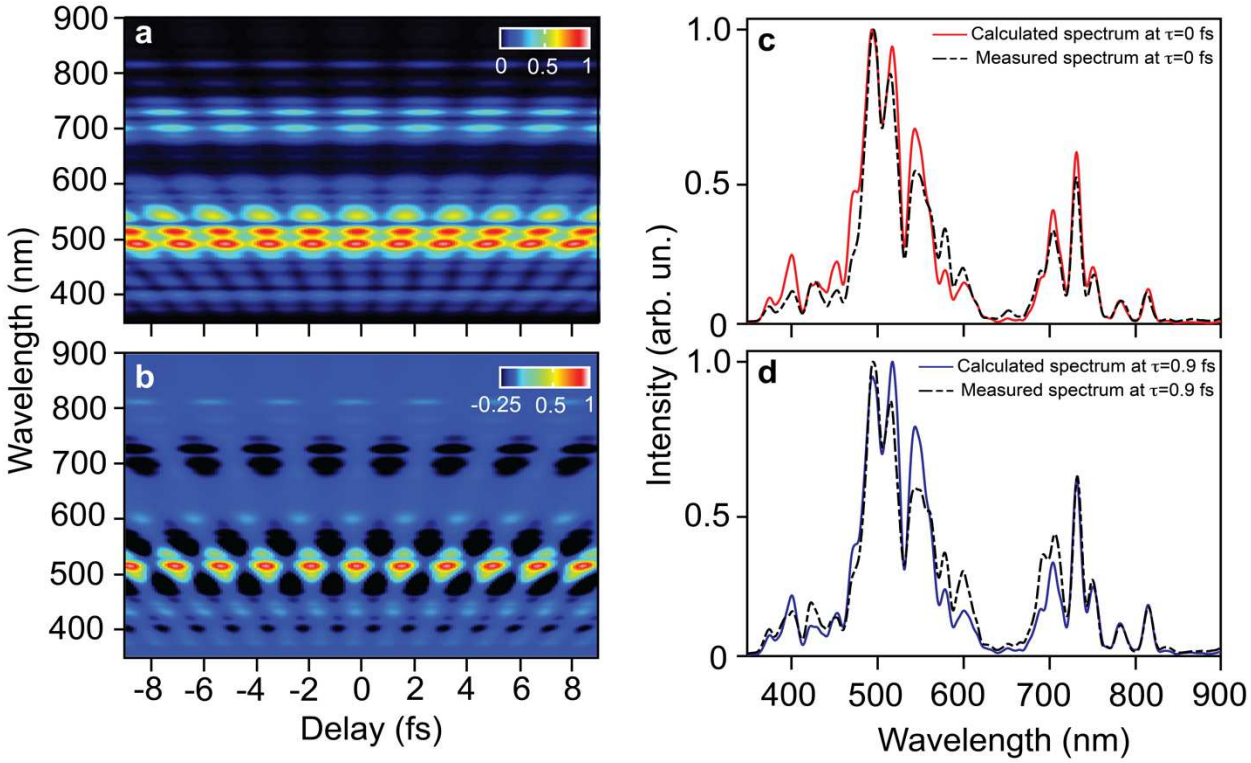

Fig. 3 | Simulated reflectivity dynamics of fused silica in a strong light field. a, The simulated spectrogram of the fused silica reflectivity modulation change in strong field using the developed simple model (see text) in frequency and time domains. **b**, The simulated spectrogram in **a** after subtracting the background spectrum (reflected spectrum in the absence of pump field). **c,** The calculated reflected spectrum at τ=0 is plotted in red solid line in contrast with the measured spectrum at same time instance which is plotted in black dashed line. **d,** The calculated and measured reflected spectra at τ=0.9 fs are plotted in blue solid and black dashed lines, respectively.

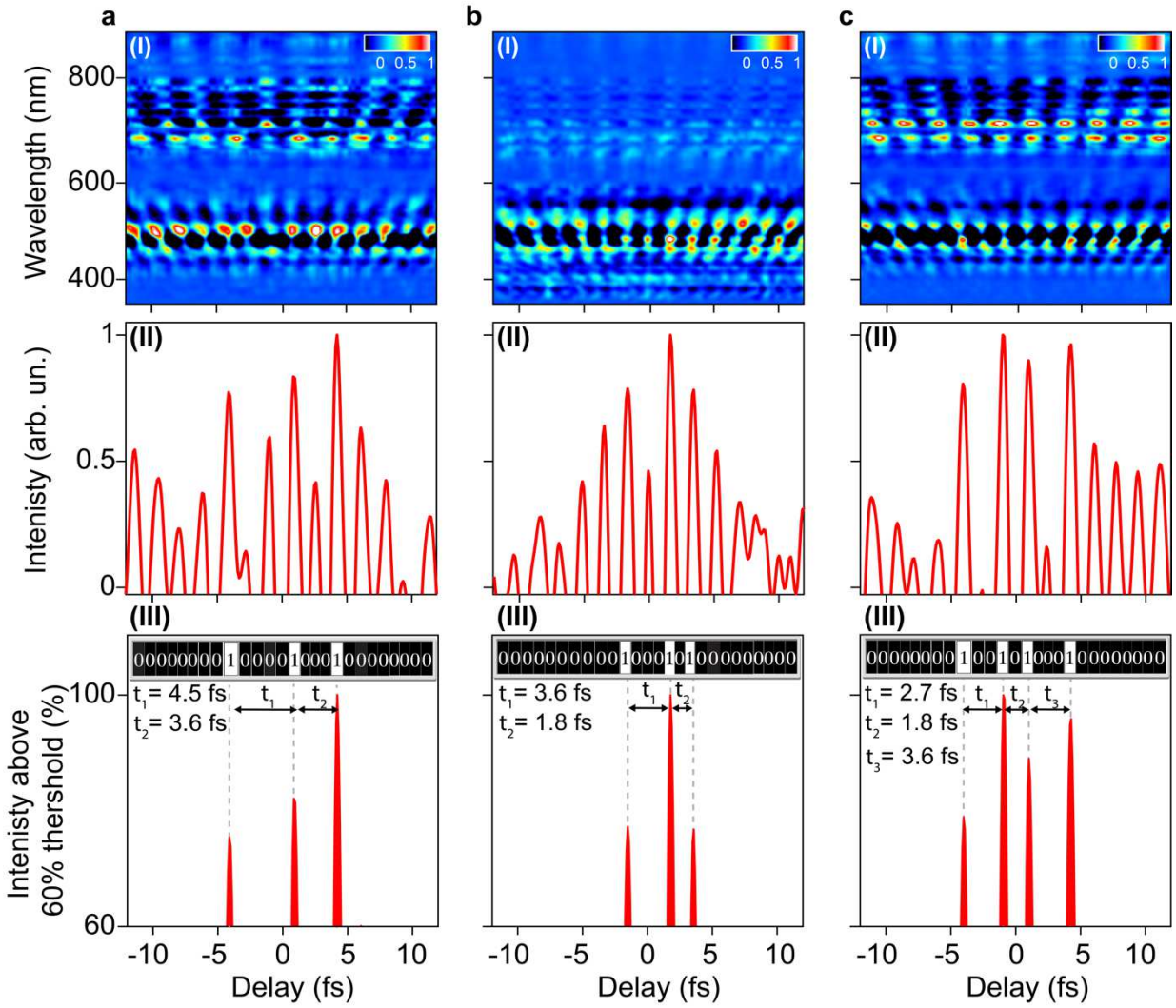

Fig. 4 | Attosecond optical switching control and ultrafast field encoding. **a (I), b (I), c (I),** The measured spectrograms of the reflected probe beam triggered by three different synthesized waveforms after subtracting the probe spectrum in the absence of the pump field. **a (II), b (II), c (II),** The positive value of the probe spectra integration as a function of time, representing the measured light signal by a photodetector in real-time, after subtracting the background. The light signal switches ON/OFF alternatively every half-cycle**. a (III), b (III), c (III),** The detected light signals above a 60% threshold. The light signals are switched ON and OFF at different time intervals. In the insets, the slots presenting the signal detection status in real-time as follows: black (0) means no signal detected above the threshold, while white (1) means the signal is above the threshold and seen by the detector. This optical switching signal control would enable the binary data encoding on light fields with petahertz and exahertz speed.

Extended data

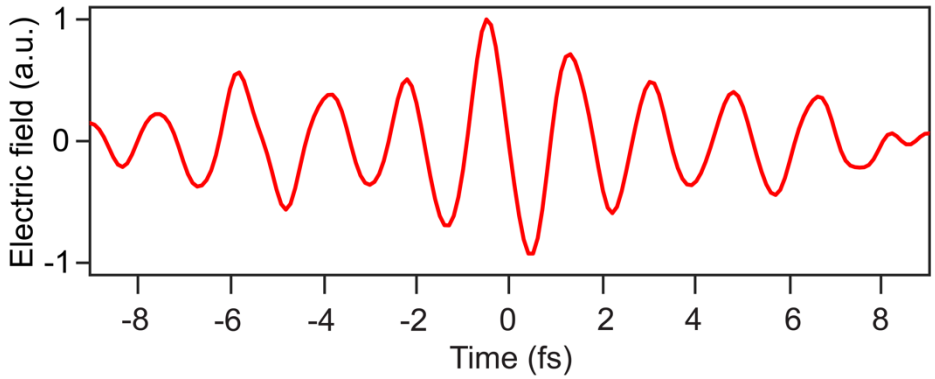

Extended Data Fig. 1. The retrieved driver electric field from the TRM trace (shown in Fig. 2c) used to induces the phase transition and the reflectivity modulation shown in Fig. 2a . This field has been also used in the simulation presented in Fig. 3a.

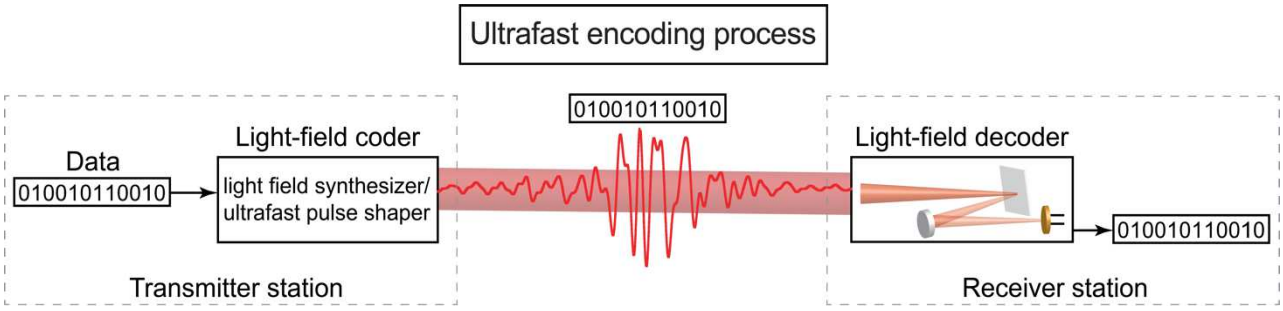

Extended Data Fig. 2. Schemitc of potential ultrafast light field encoding process exploiting the demonstrated optical switch with synthesized waveforms. The input data in the binary form (0 &1) will be sent to the light field synthesizer or the pulse shaper (encoder unit) device to tailor the field accordingly to encode the input data on the light field. The laser beam travels from the coder to the decoder unit. The data will be decoded based on measuring the reflectivity modulation of the dielectric.

Figures

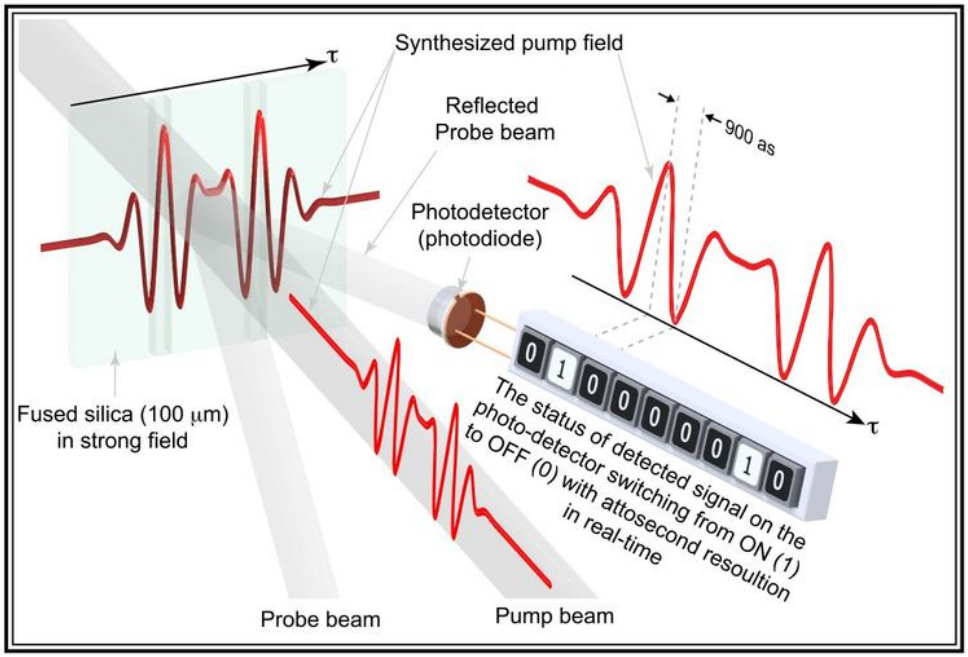

Figure 1

The basic principle of the attosecond optical switching based on strong field interaction with dielectric. The pump light field induces the instantaneous phase transition in the dielectric (fused silica) system and causes the change in the reflectivity of the dielectric following the shape of the incident pump pulse

waveform in real-time. The reflectivity modification is detected by measuring the reflected probe beam's change using a photodetector (e.g., photodiode) as a function of the time delay between pump and probe beams. The detected reflected signal is switched OFF/ON (presented by 0/1), depending on the field intensity at the time t, in the real-time. The switching resolution is equal to the duration of the half-cycle field (900 as) of the pump pulse and can be controlled by tailoring the pump field waveform using the attosecond light field synthesis approach. The attosecond optical switching and control allow to encode data on ultrafast laser pulse and open the door for establishing the ultrafast optical switchs.

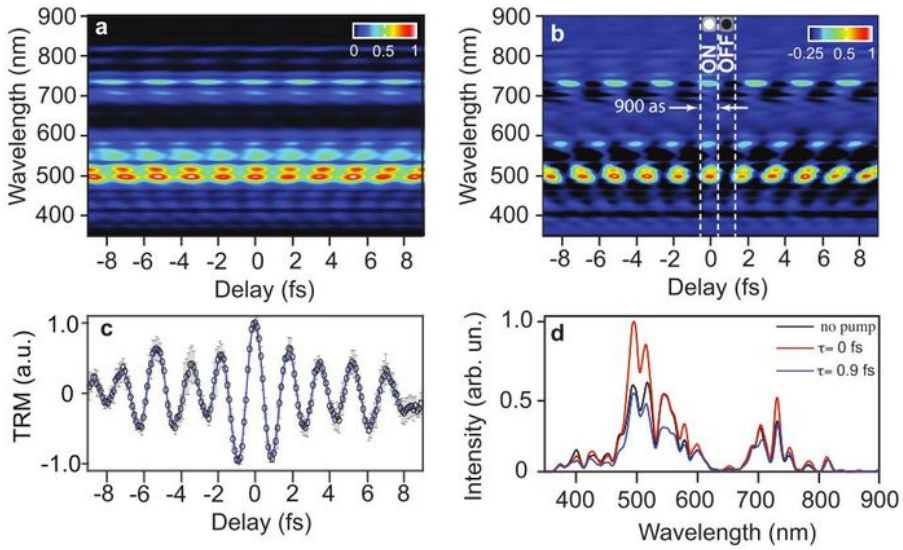

Figure 2

Attosecond optical switching. The reflectivity of SiO2 is modulated in real-time due to the interaction with a strong (pump) light field. a, The measured spectrogram (average three scans) of the reflected probe beam as a function of the time delay between the pump and probe pulses. b, The obtained spectrogram by subtracting the probe spectrum in the absence of pump field from the measured spectrogram (shown in a). The reflectivity switches between maximum to minimum alternatively in 900 attosecond time scale. c, The normalized total reflectivity modulation (TRM) of the SiO2 in the strong field retrieved obtained from the measured spectrogram (in a) by the integration of the probe spectrum at each instance of time. d, The probe beam's spectrum reflected from the SiO2 in the equilibrium state (in the absence of pump field) is shown in the black line. In contrast, reflected spectra intensities of the probe beam (outlined from the spectrogram in a) at r=0 & 0.9 fs are plotted in red and blue lines, respectively.

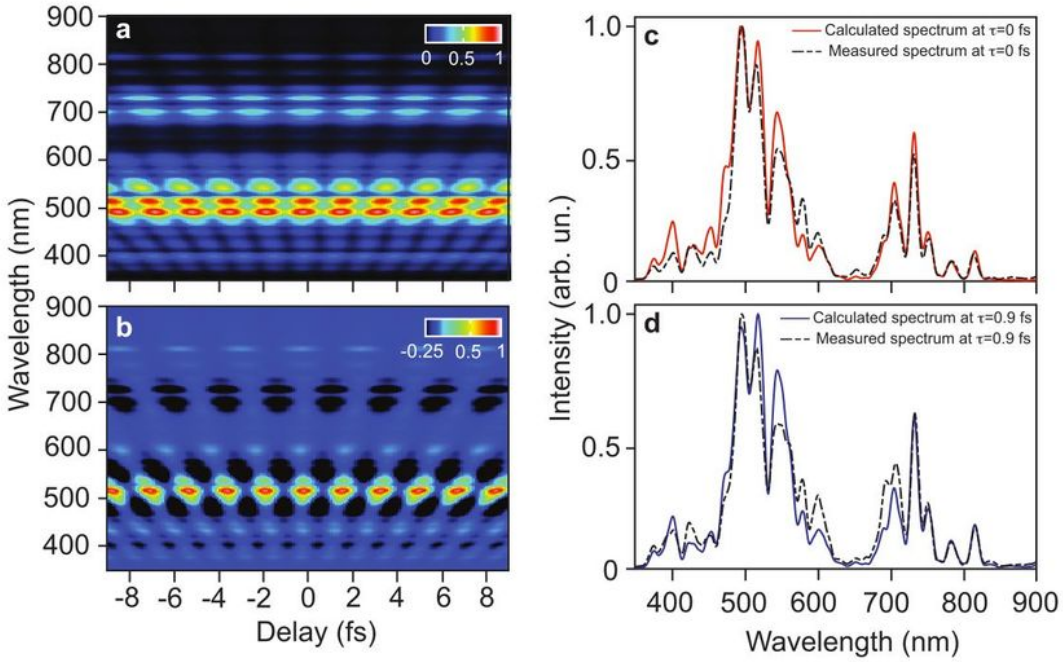

Figure 3

Simulated reflectivity dynamics of fused silica in a strong light field. a, The simulated spectrogram of the fused silica reflectivity modulation change in strong field using the developed simple model (see text) in frequency and time domains. b, The simulated spectrogram in a after subtracting the background spectrum (reflected spectrum in the absence of pump field). c, The calculated reflected spectrum at r=0 is plotted in red solid line in contrast with the measured spectrum at same time instance which is plotted in

black dashed line. d, The calculated and measured reflected spectra at r=0.9 fs are plotted in blue solid and black dashed lines, respectively.

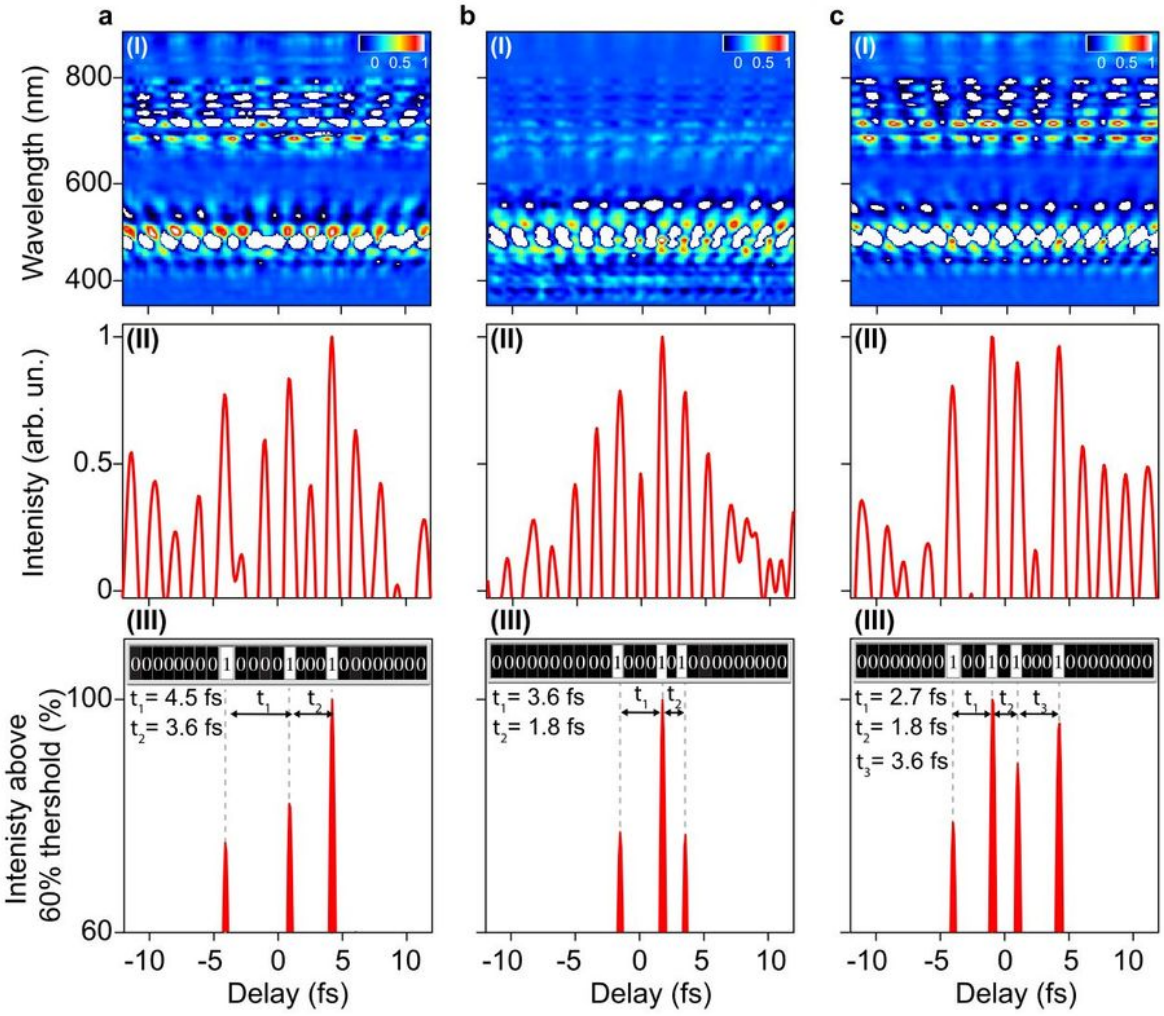

Figure 4

Attosecond optical switching control and ultrafast field encoding. a (I), b (I), c (I), The measured spectrograms of the reflected probe beam triggered by three different synthesized waveforms after

subtracting the probe spectrum in the absence of the pump field. a (II), b (II), c (II), The positive value of the probe spectra integration as a function of time, representing the measured light signal by a photodetector in real-time, after subtracting the background. The light signal switches ON/OFF alternatively every half-cycle. a (III), b (III), c (III), The detected light signals above a 60% threshold. The light signals are switched ON and OFF at different time intervals. In the insets, the slots presenting the signal detection status in real-time as follows: black (0) means no signal detected above the threshold, while white (1) means the signal is above the threshold and seen by the detector. This optical switching signal control would enable the binary data encoding on light fields with petahertz and exahertz speed.

Supplementary Files

This is a list of supplementary files associated with this preprint. Click to download.

- ExtendeddataFig.1.ai
- ExtendeddataFig.2.ai
- AttosecondOpticalSwitchingSI.pdf